Numerical Modeling of Coupled Electrochemical and Transport Processes in Lead-Acid Batteries

W. B. Gu and C. Y. Wang*

Department of Mechanical Engineering, University of Hawaii at Manoa, Honolulu, Hawaii 96822, USA

B. Y. Liaw*

Hawaii Natural Energy Institute, School of Ocean and Earth Science and Technology, University of Hawaii at Manoa, Honolulu, Hawaii 96822, USA

ABSTRACT

A numerical model is developed to predict transient behaviors of electric vehicle lead-acid batteries during discharge and charge processes. The model not only accounts for coupled processes of electrochemical kinetics and mass transport occurring in a battery cell, but also considers free convection resulting from density variations due to acid stratification. A single set of conservation equations valid for both porous electrodes and the free electrolyte region is derived and numerically solved using a computational fluid dynamics technique. This numerical methodology is capable of simulating a two-dimensional cell with the fluid flow taken into consideration and requires only tens of minutes of central processing unit time on engineering workstations. Four sample calculations are presented in this work to provide rigorous validation of the developed simulator. The simulator is capable of predicting the transient behavior of the acid concentration, the porosity of the electrodes, and the state of charge of the battery during discharge, rest, and charge cycles. The model can also be used to investigate the effects of various system parameters, such as electrode dimensions, separator design, temperature, and electrolyte composition on the battery performance (voltage, power, cold cranking amperage, etc.).

Introduction

Lead-acid batteries are widely perceived as the best near-term power source for electric vehicles (EV) due to their low cost, versatility, and excellent rechargeability and recyclability. Important characteristics of EV batteries include high specific energy and energy density, high specific power and power density, and long cycle life. The specific energy and energy density translate to the driving range of vehicles, while the specific power and power density relate to the acceleration and hill-climbing ability. A long cycle life is a key requirement if advanced EV batteries are to have reasonable life cycle costs. In order to predict and further improve these characteristics, it is important to understand the dynamic behavior of EV lead-acid batteries during discharge, rest, and charge cycles.

To complement the conventional trial-and-error method of improving the performance and cycle life of the lead-acid battery, mathematical models have been developed to predict discharge and charge behavior, as well as the effects of cycling.[1-5] Newman and Tiedemann[1] first developed a comprehensive porous electrode theory and applied it to simulate the discharge behavior of a lead-acid cell.[2] Sunu[3] proposed a similar model but included the possibility of a nonuniform concentration in the electrolyte reservoir, which was ignored by Tiedemann and Newman.[2] Gu *et al.*[4] further extended these models to predict cell behavior during discharge, rest, and charge cycles. All of these one-dimensional models, however, accounted only for variations across the cell length and thus are inherently unable to capture nonuniformities along the height of the cell.

One of the most common variations along the cell height is the nonuniform distribution of electrolyte concentration due to free convection of the electrolyte between the two electrodes. During discharge, sulfuric acid is consumed within both electrodes, and water is produced in the positive electrode. Therefore, the diluted, lighter acid close to the electrode surfaces rises, while more concentrated, and thus heavier, acid in the bulk sinks under the action of gravity. During charge, the electrochemical reaction occurs in the opposite direction, and the resulting natural convective flow reverses. The free convection caused by density variations results in a strong stratification in the free electrolyte, which may significantly affect the uniform utilization of active materials, and hence reduce battery capacity and lifetime.[6]

Most recently, Bernardi *et al.*[5] proposed a two-dimensional model to simulate the effects of the location of the electrode's current collecting tabs. Although substantial variations in current density and sulfuric acid concentration were predicted, the cell voltage averaged over the cell height was found to be closely predicted by a one-dimensional model under all practical operating conditions. However, it should be noted that free convection was not included in their work, and therefore the phenomenon of acid stratification was not addressed. On the other hand, the recent work of Alavyoon *et al.*[7] thoroughly investigated the effects of free convection and made a considerable contribution to the understanding of stratification as well as its ensuing effects on lead-acid battery performance. The work of Alavyoon *et al.*[7] was, however, restricted only to the electrolyte velocity and composition, whereas voltage characteristics were entirely ignored. Instead, a uniform current density throughout both electrodes was assumed, thus decoupling the electrochemical kinetics from the transport processes. Other assumptions made in their work included a constant electrode porosity during the electrochemical reaction.

The above literature survey shows that previous models have only considered one or more of the following aspects: (*i*) multidimensional; (*ii*) electrochemical kinetics; (*iii*) fluid flow; (*iv*) ion transfer by convection; (*v*) varying porosity of electrodes; (*vi*) variable properties; and (*vii*) cycling including discharge, rest, and charge. The objective of the present work is to develop a comprehensive battery model to incorporate all of the above elements so as to shed light on the coupled electrochemical and transport processes and to provide a more accurate prediction of dynamic performance. To this aim, an efficient and robust computational fluid dynamics (CFD) technique is employed to solve a large set of coupled, nonlinear differential equations arising from such a battery model. This numerical technique allows for fully transient simulation of battery behaviors and is thus particularly suitable for EV applications. Specific goals of this numerical work are: (*i*) to predict charge and discharge performance of lead-acid batteries and (*ii*) to identify various mechanisms limiting battery performance.

The following section describes a multidimensional mathematical model of electrochemical and transport processes occurring inside a lead-acid cell, while the third section discusses the numerical technique based on the computational fluid dynamics (CFD) approach. Several

* Electrochemical Society Active Member.

illustrative examples demonstrating various unique capabilities of this numerical model are presented in the fourth section. For model validation, extensive comparisons are also made with previous experimental and numerical results available in the literature. The last section summarizes the major conclusions from this study and future research directions.

Mathematical Model

Consider a lead-acid cell consisting of a lead dioxide electrode, an electrolyte reservoir, a porous separator, and a pure lead electrode, as schematically illustrated in Fig. 1. Each electrode is a porous, electronically conductive matrix with the pores occupied by a sulfuric acid solution. Electrical currents are applied uniformly to the left and right vertical boundaries of the unit cell shown in Fig. 1. Typical lead-acid cells have a very large aspect ratio of height to thickness, *i.e.*, the height being of the order of hundreds of millimeters and the thickness of a few millimeters.

The following electrochemical reactions occur in the two electrodes during discharge and charge, respectively

PbO_2 electrode

$$PbO_{2(s)} + HSO_4^- + 3H^+ + 2e^- \underset{\text{charge}}{\overset{\text{discharge}}{\rightleftharpoons}} PbSO_{4(s)} + 2H_2O$$

Pb electrode

$$Pb_{(s)} + HSO_4^- \underset{\text{charge}}{\overset{\text{discharge}}{\rightleftharpoons}} PbSO_{4(s)} + H^+ + 2e^-$$

Notice that PbO_2 and Pb are converted into $PbSO_4$ during discharge, and the reactions reverse during charge. Since $PbSO_4$ has a larger molar volume than both PbO_2 and Pb, the electrode pores would shrink during discharge but expand during recharge. This porosity variation is accounted for in the present model, as is elaborated below.

Two general assumptions introduced in the following model development are: (*i*) the sulfuric acid is a binary electrolyte, dissociating completely into H^+ and HSO_4^-; and (*ii*) the system is isothermal.

Model equations.—In systems consisting simultaneously of two porous electrodes and a liquid electrolyte, the total current density **i** (a vector in multidimensional situations) may generally be separated into one in the electronically conductive solid phases and the other through the ionically conducting liquid electrolyte, *i.e.*

$$\mathbf{i} = \mathbf{i}_s + \mathbf{i}_l \quad [1]$$

The assumption of electroneutrality requires that the divergence of total current density is zero, so that

$$\nabla \cdot \mathbf{i}_s + \nabla \cdot \mathbf{i}_l = 0 \quad [2]$$

which implies that the charge leaving the solid matrix must enter the pore liquid. This flux of charge is determined by the electrochemical kinetics occurring at the active material/electrolyte interface inside electrodes, *i.e.*,

$$\nabla \cdot \mathbf{i}_l = Aj \quad [3]$$

where A stands for the electroactive interfacial area per unit volume of the electrode, and the transfer current density j (from the matrix phase to the electrolyte phase) can be expressed in the general Butler-Volmer form

$$j = i_o \left(\frac{c}{c_{ref}}\right)^{\gamma} \left[\exp\left(\frac{\alpha_a F}{RT}\eta\right) - \exp\left(-\frac{\alpha_c F}{RT}\eta\right)\right] \quad [4]$$

where the overpotential η in the above kinetic equation is defined as

$$\eta = \phi_s - \phi_l - \Delta U_{PbO_2} \quad [5]$$

for the PbO_2 electrode, and as

$$\eta = \phi_s - \phi_l \quad [6]$$

for the Pb electrode. The equilibrium potential ΔU_{PbO_2} is typically a function of composition and temperature of the electrolyte and electrodes, but is taken to be constant as a first approximation. The parameters α_a and α_c are called anodic and cathodic apparent transfer coefficients, respectively. Equation 4 clearly indicates that it is the difference in the electric potentials between the solid phase and liquid electrolyte that drives electrochemical reaction and furthermore determines the transfer current between solid and electrolyte. The transfer current density is equal to zero in the electrolyte reservoir and the separator regions.

The current density in the solid phase $\mathbf{i}_s$ is proportional to the gradient of the electric potential in the solid, *i.e.*

$$\mathbf{i}_s = -\sigma^{eff} \nabla \phi_s \quad [7]$$

which follows Ohm's law. In a porous electrode, the effective conductivity of the solid matrix, σ^{eff}, differs from the solid conductivity by a correction factor accounting for the manner in which the granules of conducting phases are connected, *i.e.*

$$\sigma^{eff} = \sigma\,(1 - \epsilon)^{ex} \quad [8]$$

where σ is the solid conductivity in the absence of pores, and ϵ is the electrode porosity [*i.e.*, $(1 - \epsilon)$ is the volume fraction of the conducting solid phase]. The exponent ex is an empirically determined constant to account for the tortuosity of the solid matrix and is taken to be 1.5 in the present work. Equation 8 is usually employed as a generic correlation to calculate any effective property pertinent to porous electrodes from its material property, although the exponent ex may be different in each case.[8]

The current in the electrolytic solution is driven not only by the gradient of the electric potential but also by the concentration gradient. In a general form, one has

$$\mathbf{i}_l = -\kappa^{eff} \nabla \phi_l - \kappa_D^{eff} \nabla(\ln c) \quad [9]$$

where κ_D^{eff} is termed the "diffusion conductivity," which measures the rate of charged particle motion due to diffusion of ionic species (under the influence of a concentration gradient). Several points are worthy of noting in regard to these effective properties. First, both conductivities κ^{eff} and κ_D^{eff} are subject to corrections for the tortuosity of the porous electrode in the same way as described in

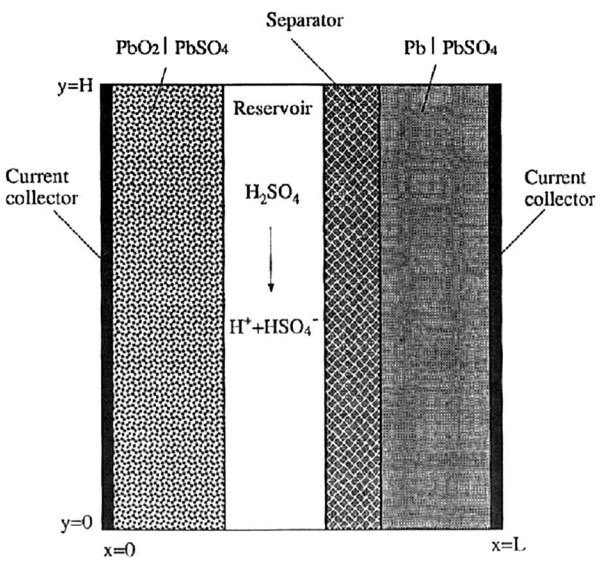

Fig. 1. Schematic illustration of a lead-acid cell and the coordinate system.

Eq. 8, except that $(1 - \epsilon)$ is replaced by ϵ.[4,8] Second, the coefficient κ^{eff} is evaluated differently for dilute and concentrated solutions. In dilute solutions, it can be shown that[8]

$$\kappa = (D_+ + D_-)cF^2/RT \quad [10]$$

whereas for concentrated solutions, κ is usually determined empirically. Last, the diffusion conductivity κ_D can be related to κ, in both cases, by

$$\kappa_D = \frac{RT\kappa}{F}(2t_+^\circ - 1) \quad [11]$$

where R denotes the gas constant, T the temperature, F Faraday constant, and t_+° the transference number of positive ionic species with respect to the solvent velocity. Equation 9 is usually termed the modified Ohm's law for the electrolyte.

Substitution of Eq. 7 and 9 into 2 and 3, respectively, yields

$$\nabla \cdot (\sigma^{eff} \nabla\phi_s) - Aj = 0 \quad [12]$$

$$\nabla \cdot (\kappa^{eff} \nabla\phi_l) + \nabla \cdot [\kappa_D^{eff} \nabla(\ln c)] + Aj = 0 \quad [13]$$

Equations 12 and 13 can be used to determine the electric potentials in the solid and liquid phases, where the source terms describe the volumetric electrochemical reaction.

A principal geometric parameter for characterizing electrode performance is the specific electroactive area A, which is, in turn, dependent upon the porosity and grain size of the electrode as well as the state of charge of the electrode. The specific electroactive area A also differs during charge and discharge because of different active materials involved. These areas can be related to the state of charge (SOC) via the following empirical relation

$$A = A_{max}\, SOC^\xi \quad [14]$$

for discharge and

$$A = A_{max}\,(1 - SOC^\xi) \quad [15]$$

for charge, where the exponent ξ is taken to be 0.55 in the present work. The state of charge SOC defined here is relative to the maximum capacity of the electrode and thus can be evaluated by the following rate equation

$$\frac{\partial(SOC)}{\partial t} = \pm\frac{\nabla \cdot \mathbf{i}_l}{Q_{max}} \quad [16]$$

where the positive and negative signs correspond to PbO_2 and Pb electrodes, respectively. The maximum available interfacial area A_{max} and the theoretical maximum capacity Q_{max} for electrochemical reaction can be obtained from the specifications of electrodes. Notice that an initial SOC value is necessary to find the solution to Eq. 16.

Another geometric parameter that dictates battery performance is the porosity of the electrode. All effective properties are strong functions of the electrode porosity (see Eq. 8), which may vary during the electrochemical reaction due to the conversion of the active solid material. The porosity change with time can be determined by

$$\frac{\partial\epsilon}{\partial t} - a_1\frac{Aj}{2F} = 0 \quad [17]$$

where the term $Aj/2F$ simply describes the flux of ionic species generated by the amount of current transfer Aj, according to the electrochemical reaction and Faraday's law, and a_1 is the coefficient accounting for the volumetric change per mole of the material converted, *i.e.*

$$a_1 = \left(\frac{M_{PbSO_4}}{\rho_{PbSO_4}} - \frac{M_{PbSO_2}}{\rho_{PbSO_2}}\right) \quad [18]$$

for the PbO_2 electrode and

$$a_1 = \left(\frac{M_{Pb}}{\rho_{Pb}} - \frac{M_{PbSO_4}}{\rho_{PbSO_4}}\right) \quad [19]$$

for the Pb electrode.

A mass balance for ionic species leads to the following conservation equation

$$\frac{\partial(\epsilon c)}{\partial t} + \mathbf{v} \cdot \nabla c = \nabla \cdot (D^{eff}\nabla c) + a_2\frac{Aj}{2F} \quad [20]$$

where mass transfer is due to convection, diffusion, and migration. Since the electrolyte is binary, the electric potential has been eliminated from Eq. 20. In such a case, the effects of migration are incorporated into the binary diffusion coefficient D^{eff}.[8] The last term on the right side of Eq. 20 represents the volumetric ion production or consumption rate where the coefficient a_2 is given by

$$a_2 = 3 - 2t_+^\circ \quad [21]$$

in the PbO_2 electrode and

$$a_2 = 1 - 2t_+^\circ \quad [22]$$

in the Pb electrode. Equation 20 reduces to the two-dimensional model of Bernardi *et al.*[5] for concentrated solutions in the absence of fluid flow. In addition, it should be noted that Eq. 20 is based on the assumption of constant transference numbers and partial molar volumes.

The motion of the liquid electrolyte is governed by the Navier-Stokes equation with the Boussinesq approximation and the continuity equation as follows

$$\frac{\partial\mathbf{v}}{\partial t} + \mathbf{v} \cdot \nabla\mathbf{v} = -\frac{1}{\rho}\nabla p + \nabla \cdot (\nu\nabla\mathbf{v}) + \mathbf{g}[1 + \beta(c - c_o)] + \frac{\nu}{K}(\epsilon\mathbf{v}) \quad [23]$$

$$\nabla \cdot \mathbf{v} = 0 \quad [24]$$

The last term in Eq. 23 is added to the Navier-Stokes equation in order to account for the drag experienced by the electrolyte flowing through open pores inside the electrode. This drag is directly proportional to the fluid viscosity and seepage velocity ($\epsilon\mathbf{v}$), and inversely proportional to the permeability of the electrode. In the case of a low-permeability electrode, the pore velocity would become so small that the inertia and viscous terms in Eq. 23 drop off, and the equation reduces to the well-known Darcy's law for flow through porous media[9]

$$\epsilon\mathbf{v} = \frac{K}{\mu}\{\nabla p - \rho\mathbf{g}[1 + \beta(c - c_o)]\} \quad [25]$$

where the permeability K is determined by Kozeny-Carman equation

$$K = \frac{\epsilon^3 d^2}{180(1 - \epsilon)^2} \quad [26]$$

with ϵ and d being the porosity and mean diameter of particles making up the electrode. For a typical electrode with $\epsilon \approx 0.5$ and $d \approx 0.1$ μm, one finds that $K \approx 5 \times 10^{-15}$ m^2. This magnitude of permeability will render the electrolyte inside electrode pores practically stagnant. This leaves the ion transport within electrodes by diffusion and migration only. On the other hand, in the electrolyte reservoir, the permeability K approaches infinity because the porosity is equal to unity (see Eq. 26); thus, the additional drag term vanishes and Eq. 23 recovers the original Navier-Stokes equation. Therefore, Eq. 23 is generally applicable throughout the cell, including porous electrodes, electrolyte reservoir, and separator.

The above mathematical model consisting of Eq. 12, 13, 20, 23, and 24 provides a sufficient set of equations to

determine five primary unknowns: (*i*) potential in the solid matrix, ϕ_s; (*ii*) potential in the liquid electrolyte, ϕ_l; (*iii*) concentration of sulfuric acid, *c*; (*iv*) velocity vector, **v**; and (*v*) pressure in the liquid solution, *p*. In addition, the model can determine the electrode porosity evolution and battery state of charge, which are crucial for design and application of batteries. It should be noted that the present model equations are highly coupled with one another and exhibit strong nonlinearities. For example, solid and liquid potentials are interlinked through the transfer current density *j* which is, in turn, determined by the overpotential, ϕ_s-ϕ_l. The transfer current density is also a strong function of the acid concentration; see Eq. 4. The sulfuric acid concentration is computed from the species balance equation, Eq. 20, by knowing the transfer current density, *j*. The acid concentration is also affected by the fluid motion which results, in turn, from the concentration gradients and hence density variations. The present work aims at developing an efficient numerical methodology to solve this highly coupled set of nonlinear equations governing electrochemistry and transport processes in a multidimensional system.

Initial/boundary conditions.—To close the mathematical system, initial/boundary conditions for the primary variables are necessary. The potentials in the solid and liquid phases are governed by Poisson equations without time derivatives; hence, their initial conditions are not necessary. The appropriate boundary conditions for ϕ_s and ϕ_l are

$$\frac{\partial \phi_l}{\partial \mathbf{n}} = \frac{\partial \phi_s}{\partial \mathbf{n}} = 0 \qquad [27]$$

everywhere on the cell boundaries except for the ones where the current is collected. Here, **n** is the unit vector normal to the boundary surface. On the collector surfaces, the boundary condition becomes

$$\phi_s = 0 \text{ or } V \qquad [28]$$

for a given voltage, or

$$-\sigma^{\text{eff}} \frac{\partial \phi_s}{\partial \mathbf{n}} = I \qquad [29]$$

for a prescribed current density. Positive values of *I* refer to charging, whereas negative values of *I* denote discharging.

Because the battery cell is a closed system, the concentration boundary condition is simply given by

$$\frac{\partial c}{\partial \mathbf{n}} = 0 \qquad [30]$$

and its initial condition corresponds to a given initial acid concentration, *i.e.*

$$c = c_o \qquad [31]$$

Model discussion.—Several salient features of the present model are worth noting. First, to the authors' knowledge, this numerical model is the first one that fully integrates electrochemical kinetics, mass transport, fluid flow, and multidimensional aspects of a battery system. The present model extends the two-dimensional model of Bernardi *et al.*[5] by including fluid flow and acid stratification, and Alavyoon *et al.*'s model[7] by fully coupling the electrochemistry with the transport processes.

Second, the present model does not distinguish between dilute and concentrated solutions. In other words, a single set of model equations is equally applicable to both dilute and concentrated solutions, while leaving the descriptions of different electrochemistry and transport characteristics of each solution system to supplementary relations. For example, using Eq. 10 to evaluate the electrolyte conductivity κ, the governing equations would reduce to the dilute solution theory.[8] In the other limit where κ is determined empirically, the present set of governing equations then becomes identical to the concentrated solution models of Bernardi *et al.*[5] and Nguyen *et al.*[10]

Third, it should be noted that all the governing equations in the present model, Eq. 12, 13, 20, 23, and 24, are equally applicable in various regions like electrodes, electrolyte reservoir, and separator. Matching conditions between different regions thus become unnecessary. This is in contrast to the multidomain approach used in virtually all previous modeling work,[2,4,5] where different governing equations are written for each region, and matching conditions at the interface between two adjacent regions are required. Apparently, the present single-domain formulation offers considerable simplifications in numerical simulation.

Numerical Procedures

To solve the foregoing model equations numerically, the general CFD methodology is adopted. The key to a successful application of CFD techniques is that all the equations in the present battery model can be cast into a general form of convection-diffusion type, *i.e.*

$$\underbrace{\frac{\partial \Phi}{\partial t}}_{\text{transient}} + \underbrace{\nabla \cdot (\mathbf{v}\Phi)}_{\text{convection}} = \underbrace{\nabla \cdot (\Gamma \nabla \Phi)}_{\text{diffusion}} + \underbrace{S}_{\text{source}} \qquad [32]$$

where Φ is a general variable to be solved, Γ a diffusion coefficient, and *S* a source term which includes all terms that cannot be included in the previous terms. Various expressions for Γ and *S* corresponding to each model equation are given in Table I.

The general differential equation is discretized by the control-volume-based finite difference method of Patankar,[11] and the resulting set of algebraic equations is iteratively solved. The numerical solver for the general differential equation can be repeatedly applied for each scalar variable over a control volume mesh. The solution of each component of the Navier-Stokes equation is, however, obtained in a staggered control volume; see Ref. 11 for details. In addition, there exists a fundamental difficulty in the calculation of the velocity field as related to the appearance of the (unknown) pressure gradient in the Navier-Stokes equation. This is overcome by the so-called

Table I. Summary of model equations and their numerical implementation.

Equation	Transient term	Diffusion coefficient, Γ	Source term, *S*, in Eq. 32
Conservation of charge in solid: $\nabla \cdot (\sigma^{\text{eff}} \nabla \phi_s) - Aj = 0$	No	σ^{eff}	$-Aj$
Conservation of charge in liquid: $\nabla \cdot (\kappa^{\text{eff}} \nabla \phi_l) + \nabla \cdot [\kappa_D^{\text{eff}} \nabla(\ln c)] + Aj = 0$	No	κ^{eff}	$\nabla \cdot [\kappa_D^{\text{eff}} \nabla(\ln c)] + Aj$
Species (ionic) conservation: $\frac{\partial(\epsilon c)}{\partial t} + \mathbf{v} \cdot \nabla c = \nabla \cdot (D^{\text{eff}} \nabla c) + a_2 \frac{Aj}{2F}$	Yes	D^{eff}	$a_2 \frac{Aj}{2F} + (1 - \epsilon) \frac{\partial c}{\partial t} - c \frac{\partial \epsilon}{\partial t}$
Momentum conservation: $\frac{\partial \mathbf{v}}{\partial t} + \mathbf{v} \cdot \nabla \mathbf{v} = -\frac{1}{\rho} \nabla p + \nabla \cdot (\nu \nabla \mathbf{v}) + \mathbf{g}[1 + \beta(c - c_o)] + \frac{\nu}{K}(\epsilon \mathbf{v})$	Yes	ν	$\mathbf{g}[1 + \beta(c - c_o)] + \frac{\nu}{K}(\epsilon \mathbf{v})$

Table II. Properties used in numerical simulations.

Electrolyte	
Diffusion coefficient, D, cm^2/s	
$D = (1.75 + 260.0c)(10^{-5}) \exp\left(\frac{2174.0}{298.15} - \frac{2174.0}{T}\right)$	
Conductivity, κ, S/cm	
$\kappa = c \exp(1.1104 + (199.475 - 16097.781c)\, c + (3916.95 - 99406.0c - 712860.0/T)/T]$	
Kinematic viscosity, ν, cm^2/s	10^{-2}
Volume expansion coefficient, β, cm^3/mol	35.0
PbO_2	
Conductivity, σ, S/cm	80
Density, ρ, g/cm^3	9.7
Pb	
Conductivity, σ, S/cm	4.8×10^4
Density, ρ, g/cm^3	11.34
$PbSO_4$	
Density, ρ, g/cm^3	6.3

semi-implicit method for pressure-linked equations revised (SIMPLER) algorithm developed by Patankar.[11]

The rectangular physical domain is divided by either a uniform or nonuniform grid consisting of m horizontal and n vertical grid lines. Stringent numerical tests were performed in every case to ensure that the solutions were independent of the grid size and time step. For the examples to be illustrated below, it was found that the typical number of grid lines across the cell width was about 60, while a similar number of gridlines was needed along the height direction in two-dimensional simulations. The equations are solved as a simultaneous set, and convergence is considered to be reached when the relative error in each field between two consecutive iterations is less than 10^{-6}. A typical transient simulation for one- and two-dimensional problems required about 10 s and 30 min, respectively, of CPU time on an HP715/75 workstation. Such central processing unit (CPU) time is quite manageable and will permit a full simulation of the dynamic behavior of EV batteries involving hundreds of charge and discharge cycles.

Illustrative Examples

In this section, the capabilities of the present model are illustrated through three "benchmark" cases that have been widely studied in the literature. These cases correspond to three different cells and four simulations. The material properties used in these simulations are summarized in Table II. The diffusion coefficient, D, and conductivity, κ, of the electrolyte are concentration- and temperature-dependent and calculated according to the empirical expressions of Tiedemann and Newman,[2] while other properties are assumed to be constant and taken from the work of Gu *et al.*[4] and Alavyoon *et al.*[7] The input parameters for different cells or simulations are listed in Table III. The first cell corresponds to the experimental work of Tiedemann and Newman,[2] in which most of the input parameters are experimental data and therefore used directly in the present simulation. The second cell corresponds to the one-dimensional discharge and charge simulations of Gu *et al.*[4] Their simulation results were reportedly to be in good agreement with General Motors' experimental data, and thus are chosen to indirectly validate the present simulator. The input parameters identical to those in Gu *et al.*[4] are presented in Table III, where some individual parameters may not be realistic, but collectively produced realistic cell voltages. The third cell corresponds to the experimental work of Alavyoon *et al.*,[7] where electrolyte velocity and concentration in the reservoir region were measured. The electrokinetic parameters for this cell were not available and are reasonably estimated in the present study. It should also be mentioned that in the third cell, cell charge was intentionally performed at a low current density, thereby allowing sufficient time for acid stratification and fluid flow to develop. This third simulation thus requires application of a full version of the foregoing simulator in a two-dimensional situation.

Discharge.—One-dimensional discharge processes for cells 1 and 2, given in Table III, are simulated. The discharge process for cell 1 occurs at 21.7°C and at two low current densities of 10 and 40 mA/cm^2 as experimentally and theoretically studied by Tiedemann and Newman,[2] while the discharge process for cell 2 occurs at 25°C and at a higher current density of 340 mA/cm^2 as studied by Gu *et al.*[4] For cell 1, the predicted cell voltage is plotted in Fig. 2 as a function of the charge density (*i.e.*, the product of current density and discharge time), where the corresponding experimental data of Tiedemann and Newman[2] are also shown. It can be seen that the numerical results agree with the experimental data except for the initial period during which the experimental data indicates a

Table III. Input parameters to numerical simulations.

	Cell 1	Cell 2	Cell 3
Geometrical			
Cell height, cm	—	—	3.2
PbO_2 electrode width, cm	0.0865	0.06	0.2
PbO_2 electrode porosity	0.55	0.53	0.5
Reservoir width, cm	0.16	0.055	0.2
Separator width, cm	0.056	0.014	0
Separator porosity	0.60	0.73	—
Pb electrode width, cm	0.0815	0.06	0.2
Pb electrode porosity	0.61	0.53	0.5
Chemical and thermal			
Initial acid concentration, mol/cm^3	4.8×10^{-3}	4.9×10^{-3}	2×10^{-3}
Operating temperature, °C	21.7	25	25
Electrokinetic			
Transfer number of H^+	0.9	0.72	0.8
Exchange current density, mA/cm^2			
PbO_2 electrode	6×10^{-4}	10	0.1
Pb electrode	8×10^{-3}	10	0.1
Maximum electroactive area, cm^2/cm^3			
PbO_2 electrode	20.5×10^4	100	100
Pb electrode	2.5×10^4	100	100
Maximum capacity (charged state), C/cm^3			
PbO_2 electrode	2800	5660	3130
Pb electrode	2471	5660	3700
Exponent in Eq. 4, γ			
PbO_2 electrode	0.5	1.5	1.5
Pb electrode	0.5	1.5	1.5
Apparent transfer coefficient, $\alpha = \{\alpha_a, \alpha_c\}$			
PbO_2 electrode	0.7, 1.3	0.5, 0.5	1.0, 1.0
Pb electrode	1.0, 1.0	0.5, 0.5	1.0, 1.0
Applied current density, mA/cm^2	−10, −40	−340, 20	9.434

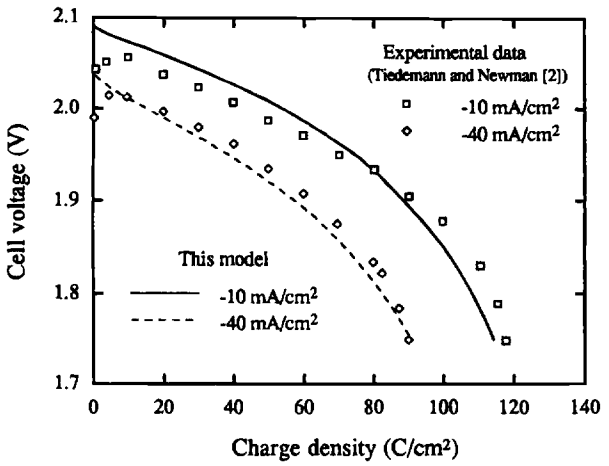

Fig. 2. A comparison of experimental and predicted cell voltage *vs.* charge density (current density times discharge time) at constant current discharge.

slight rise of the cell voltage. This behavior is contributed to the so-called *coup de fouet* or voltage-dip phenomenon[12] and is not included in the present model. For cell 2, the discharge curve predicted by the present model is shown in Fig. 3a, together with the corresponding results of Gu *et al.*[4] It can be seen that there is good agreement between the two predictions. The time to the voltage cutoff (*i.e.*, 1.55 V) is predicted to be approximately 106 s. The acid concentration profile at this time, as shown in Fig. 3b, clearly indicates that the end of discharge is caused by the acid depletion inside the PbO_2 electrode, where acid is consumed at a greater rate than in the Pb electrode. This set of simulations establishes the capability and accuracy of the present model in simulating the discharge behavior of EV lead-acid batteries.

Charge.—A charge simulation for cell 2 is conducted following a discharge at −18°C and 340 mA/cm² to a cutoff of 1.55 V, and a rest period of 1 h at −18°C. The charge is then performed at 25°C and 20 mA/cm². The entire series of discharge, rest, and charge is simulated using the foregoing model, and the predicted cell voltage and concentration profiles in the charge portion are shown in Fig. 4a and b. The present results compare well to those of Gu *et al.*[4] in terms of both cell voltage and acid concentration. Note also that the concentration of electrolyte is relatively uniform at the end of 1 h rest (*i.e.*, $t = 0$), indicating the importance of rest for rapid and efficient charge. This simulation was performed to validate the capability of the present model in predicting battery behavior during a complete cycle of discharge, rest, and charge.

In practice, lead-acid batteries may also be charged under a constant potential with a current limit. This boundary condition is readily implemented in the present model (see Eq. 28). In contrast, in previous models the

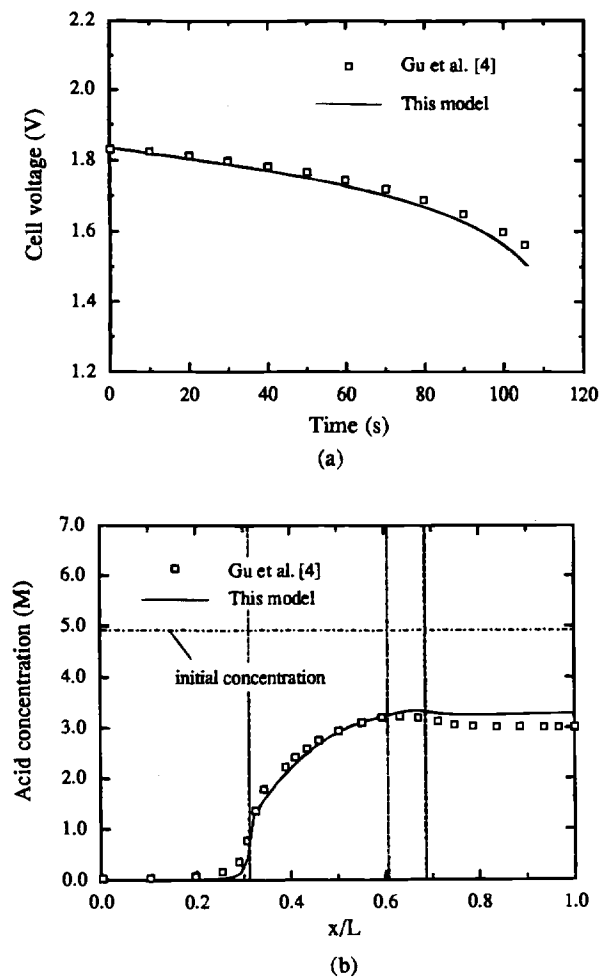

Fig. 3. Discharge behavior at 25°C and the current density of 340 mA/cm²: (a) cell voltage curve and (b) acid concentration profile at $t = 106$ s. Comparison between the present model and the model of Gu *et al.*[4]

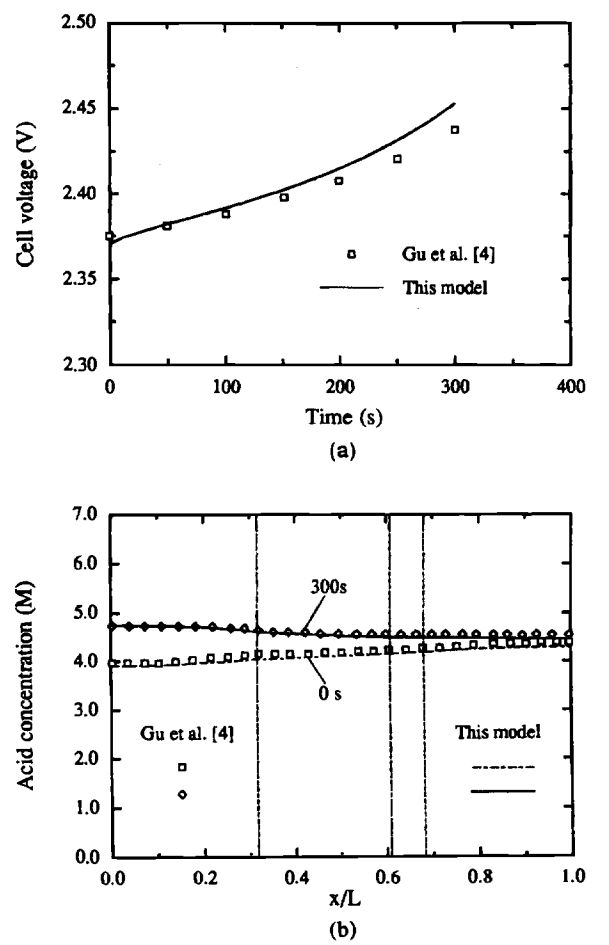

Fig. 4. Charge behavior at 25°C and the current density of 20 mA/cm²: (a) cell voltage curve and (b) acid concentration profile at $t = 300$ s. Comparison between the present model and the model of Gu *et al.*[4]

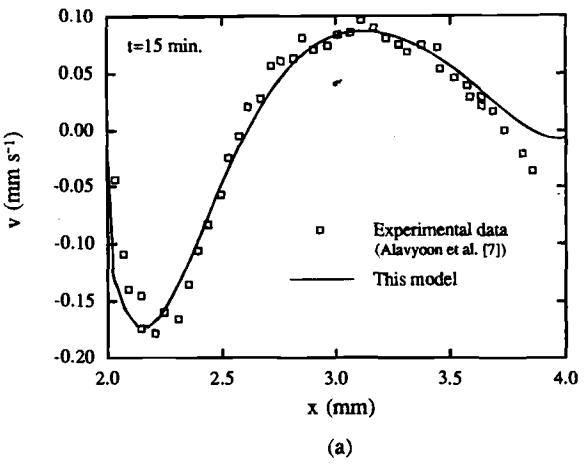

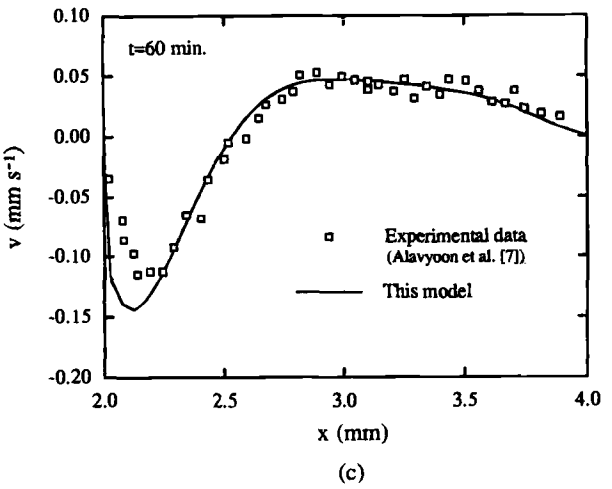

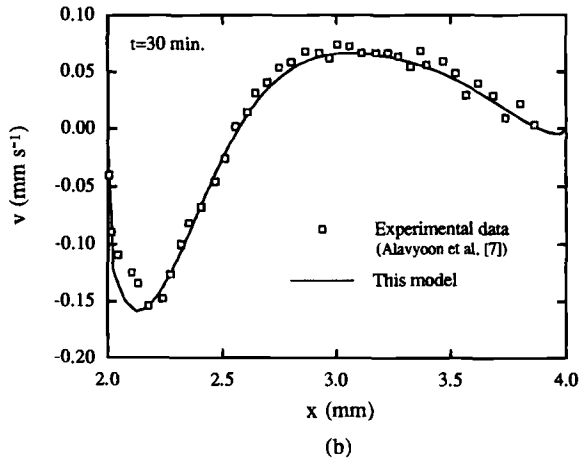

Fig. 5. Comparison of predicted and measured vertical velocity profiles at the half height of the electrolyte reservoir during charge at the current density of 9.434 mA/cm²: (a) t = 15 min, (b) t = 30 min, and (c) t = 60 min. x = 2.0 mm denotes the boundary between PbO_2 electrode and reservoir, while x = 4.0 mm stands for the boundary between reservoir and Pb electrode.

charging condition was implemented through iterating the applied charging current to yield the given potential.[4]

Acid stratification during charge.—To test the full capabilities of the model featuring two-dimensional effects and fluid flow, a slow charge experiment is simulated in this subsection. The experiment was performed by Alavyoon *et al.*,[7] in which a lead-acid cell with the initial acid concentration of 2×10^{-3} mol/cm³ was recharged at the current density of 9.434 mA/cm². Note that this current density is markedly lower than that in the charge simulation of the second cell, thus free convection and resulting acid stratification are rather pronounced. Alavyoon *et al.*[7] used laser doppler velocimetry (LDV) and holographic laser interferometry (HLI) to measure velocity and concentration distributions in the reservoir region, respectively. These experimental data are compared with the present numerical predictions in Fig. 5 and 6.

Figure 5 shows the profiles of the vertical component of the velocity vector across the free electrolyte between the electrodes at the half height of the cell at various times of charging, *i.e.*, t = 15, 30, and 60 min. It can be seen that, in the charge process, the electrolyte adjacent to the electrodes becomes heavier due to acid production and hence moves downward. Due to the requirement of mass conservation, there is an upward motion of the electrolyte in the middle of the cell. The maximum velocity near the PbO_2 electrode is significantly larger than that near the Pb electrode, simply because the rate of acid production is much higher in the PbO_2 electrode than in the Pb electrode. These figures also demonstrate good agreement between calculated and measured velocity profiles.

Figure 6 compares the acid concentration profiles measured by Alavyoon *et al.*[7] and predicted by the present model along a vertical cross section in the middle of the free electrolyte region for t = 15, 30, and 60 min. Agreement is once again reasonably good. In particular, the acid stratification effect (reflected as an inclined curve instead of a vertically straight line in Fig. 6) is successfully captured. Such an effect may lead to inefficient material utilization and limited performance, thus reducing life time of the battery.

Figure 7 displays two-dimensional contour plots of the predicted acid concentration field throughout the cell,

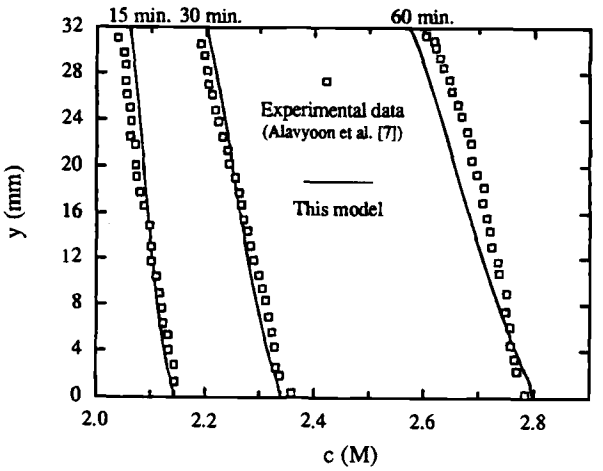

Fig. 6. Comparison of predicted and measured vertical concentration profiles in the middle of the electrolyte reservoir during charge at the current density of 9.434 mA/cm² for t = 15, 30, and 60 min.

including both porous electrodes. The central part of the isopleths in each plot of Fig. 7, which covers the free electrolyte reservoir, clearly illustrates the acid stratification effect. Moreover, acid stratification becomes more and more severe into the charge process.

Conclusions

A comprehensive battery model has been developed to simulate the dynamic behavior of EV lead-acid batteries during cycles of discharge, rest, and charge. The model

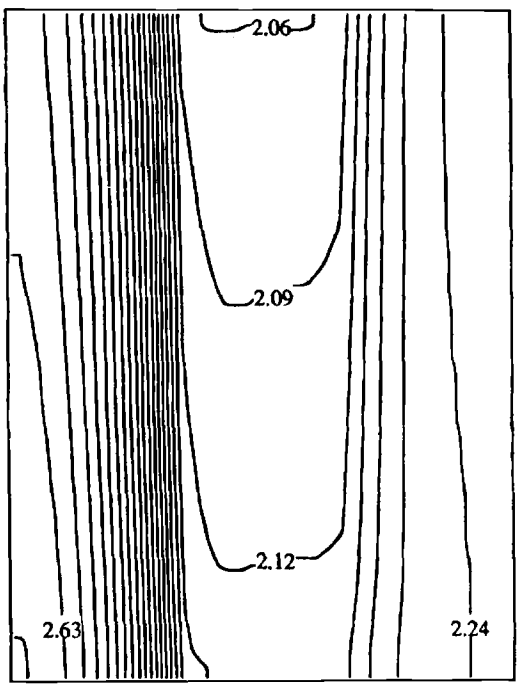

(a) t=15 min.

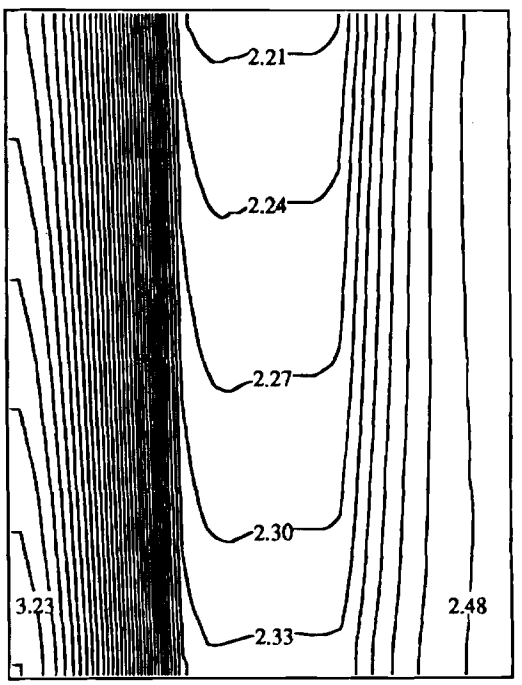

(b) t=30 min.

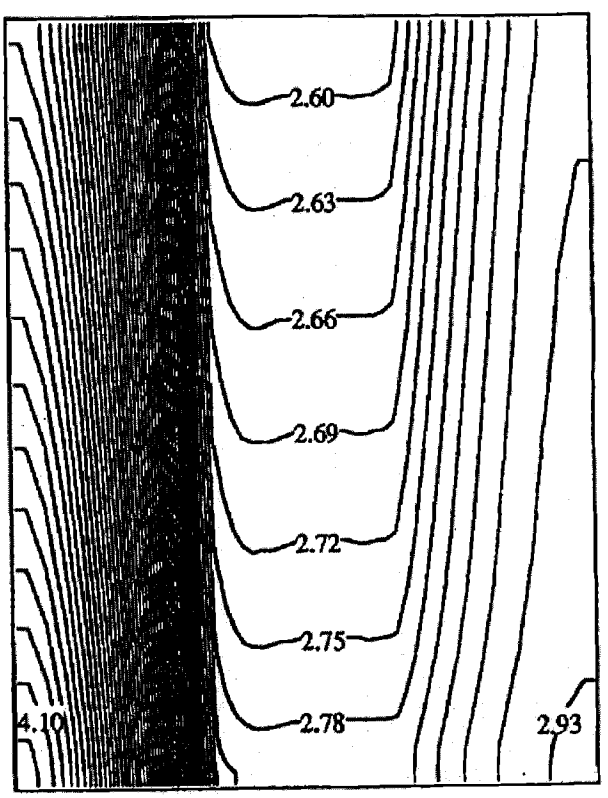

(c) t=60 min.

Fig. 7 Predicted contours of acid concentration throughout the cell during charge at the current density of 9.434 mA/cm²: (a) t = 15 min, c_{max} = 2.66 M, c_{min} = 2.06 M, (b) t = 30 min, c_{max} = 3.26 M, c_{min} = 2.21 M, and (c) t = 60 min, c_{max} = 4.13 M, c_{min} = 2.60 M with the same increment of Δc=0.03 M. The maximum concentration is located in the lower left corner (*i.e.*, PbO_2 electrode), while the minimum concentration appears in the upper middle region (*i.e.*, electrolyte reservoir).

features intimate couplings of electrochemical kinetics and transport processes. In addition, fluid flow has been incorporated, thus rendering the model capable of addressing free convection and acid stratification phenomena. Adopting a CFD technique, numerical simulation of a full battery system has been made possible with reasonable CPU time on engineering workstations. Such an efficient approach will allow for a full evaluation of EV lead-acid batteries undergoing many hundreds of cycles. The efficiency of this numerical model is more impressive in situations where only a simplified version of the model (*e.g.*, in one-dimensional cases) is adequate.

The present model has been carefully validated in three benchmark cases (both experimental and theoretical). Good agreement in all cases has been achieved. Efforts are currently underway to validate the present simulator further against battery data collected at our battery testing laboratory and to use the model to understand fundamental mechanisms involved in sophisticated driving cycles and pulsed charging techniques.

Acknowledgments

This work is partly supported by the Defense Advanced Research Projects Agency (DARPA) through the Hawaii Electric Vehicle Demonstration Project (HEVDP). The authors are grateful to Dr. David Yun for many stimulating discussions throughout this work.

Manuscript submitted Dec. 5, 1996; revised manuscript received Feb. 25, 1997.

The University of Hawaii at Manoa assisted in meeting the publication costs of this article.

LIST OF SYMBOLS

a	coefficient
A	specific electroactive area, cm^2/cm^3
c	acid concentration, mol/cm^3
d	mean diameter of electrode particles, μm
D	diffusion coefficient, cm^2/s
ex	exponent in the effective property
F	Faraday constant, 96,487 C/eq
$\mathbf{g}$	gravitational vector, $9.81\ m/s^2$
H	cell height, cm
i_o	exchange current density, mA/cm^2
$\mathbf{i}$	current density vector, mA/cm^2
I	applied current density, mA/cm^2
j	transfer current density, mA/cm^2
K	permeability, cm^2
L	cell width, cm
M	molecular weight, kg/kmol
$\mathbf{n}$	unit vector normal to a boundary surface
p	pressure, Pa
Q	electrode capacity, C/cm^3
R	universal gas constant, 8.3143 J/mol K
S	source term
SOC	state of charge
t	time, s
T	absolute temperature, K
t_+^o	transference number of H^+ relative to the solvent
ΔU_{PbO_2}	thermodynamic open-circuit cell potential, V
$\mathbf{v}$	velocity vector, cm/s
x	normal distance from the center of the PbO_2 electrode, cm
y	distance from the bottom of the cell, cm

Greek

α	transfer coefficient
β	volume expansion coefficient, cm^3/mol
γ	exponent for the concentration dependence of the exchange current density
Γ	diffusion coefficient
ϵ	porosity
ξ	exponent for charge dependence of the specific electroactive area
η	electrode overpotential, V
κ	electrolyte conductivity, S/cm
μ	dynamic viscosity, kg/cm s
ν	kinematic viscosity, cm^2/s
ρ	density, g/cm^3
σ	conductivity of the solid matrix, S/cm
ϕ	electric potential, V
Φ	general variable in Eq. 32

Subscripts

D	pertinent to diffusion
l	liquid solution
max	maximum or theoretical
o	initial value
ref	reference state
s	solid phase

Superscripts

eff	effective, corrected for tortuosity

REFERENCES

1. J. Newman and W. Tiedemann, *AIChE J.*, **21,** 25 (1975).
2. W. Tiedemann and J. Newman, in *Battery Design and Optimization*, S. Gross, Editor, PV 79-1, p. 23, The Electrochemical Society Proceedings Series, Princeton, NJ (1979).
3. W. G. Sunu, in *Electrochemical Cell Design,* R. E. White, Editor, p. 357, Plenum Press, New York (1984).
4. H. Gu, T. V. Nguyen, and R. E. White, *This Journal,* **134,** 2953 (1987).
5. D. M. Bernardi, H. Gu, and A. Y. Schoene, *ibid.*, **140,** 2250 (1993).
6. W. G. Sunu and B. W. Burrows, *ibid.*, **128,** 1405 (1981).
7. F. Alavyoon, A. Eklund, F. H. Bark, R. I. Karlsson, and D. Simonsson, *Electrochim. Acta,* **36,** 2153 (1991).
8. J. Newman, *Electrochemical Systems,* Prentice Hall, Englewood, NJ (1991).
9. J. Bear, *Dynamics of Fluids in Porous Media,* Elsevier, New York (1972).
10. T. V. Nguyen, R. E. White, and H. Gu, *This Journal,* **137,** 2998 (1990).
11. S. V. Patankar, *Numerical Heat Transfer and Fluid Flow, Hemisphere,* Washington DC (1980).
12. H. Bode, *Lead-Acid Batteries,* R. J. Brodd and Karl V. Kordesch, Translators, John Wiley & Sons, New York (1977).